

Manuscript Number: APEN-D-16-06037

Title: Thermochemical Energy Storage with CaO/Ca(OH)<sub>2</sub> - Experimental investigation of the thermal capability at low vapor pressures in a lab scale reactor

Article Type: Research Paper

Keywords: thermochemical energy storage;  
calcium hydroxide;  
calcium oxide;  
operation modes;  
low vapor pressures;  
thermal charging and discharging

Corresponding Author: Mr. Matthias Schmidt, Dipl.-Ing.

Corresponding Author's Institution: German Aerospace Center

First Author: Matthias Schmidt, Dipl.-Ing.

Order of Authors: Matthias Schmidt, Dipl.-Ing.; Andrea Gutierrez; Marc Linder, Dr.

Abstract: The reversible reaction of calcium hydroxide (Ca(OH)<sub>2</sub>) to calcium oxide (CaO) and water vapor is well known in the context of thermochemical energy storage. Cheap material costs, a theoretically very high energy density and the potentially wide temperature range of the reaction imply that the storage system could be beneficial for many high temperature processes. For example the system could be applied to store and reutilize industrial waste heat or as an alternative storage solution in future concentrated solar power plants.

In this publication the reaction is experimentally investigated in an indirectly operated reactor at different technically relevant but so far not investigated operating conditions. This in particular means the thermal charging and discharging of the storage at low water vapor pressures under different heating and cooling loads induced by a heat transfer fluid. The experiments revealed that the reaction gas handling not only affects the operating range of the storage but has also a significant influence on its thermal capability. Especially at low vapor pressures operational limits of the system have been identified and could be contributed to the effective reaction rate of the unmodified reaction material which is in the relevant operating range very sensitive to small changes of the local reaction conditions.

## Highlights

Development of a novel indirectly heated reaction bed for thermochemical energy storage

Experimental demonstration of thermal charging and discharging at low vapor pressures (1.4 – 20 kPa)

Experimental study of the reaction at various heating and cooling loads of the heat transfer fluid

Identification of operational limits under some technically relevant boundary conditions

1 **Thermochemical Energy Storage with CaO/Ca(OH)<sub>2</sub> – Experimental investigation of the**  
2 **thermal capability at low vapor pressures in a lab scale reactor**  
3

4 **Matthias Schmidt<sup>1</sup>, Andrea Gutierrez<sup>2</sup>, Marc Linder<sup>2</sup>**

5 <sup>1</sup>German Aerospace Center – DLR e.V., Institute of Technical Thermodynamics, Linder Höhe, 51147 Köln, Germany

6 <sup>2</sup>German Aerospace Center – DLR e.V., Institute of Technical Thermodynamics, Pfaffenwaldring 38, 70569 Stuttgart, Germany

7 Corresponding author: Matthias Schmidt, Matthias.schmidt@dlr.de

8 **Highlights**

9 Development of a novel indirectly heated reaction bed for thermochemical energy storage

10 Experimental demonstration of thermal charging and discharging at low vapor pressures (1.4 – 20  
11 kPa)

12 Experimental study of the reaction at various heating and cooling loads of the heat transfer fluid

13 Identification of operational limits under some technically relevant boundary conditions

14 **Keywords:** thermochemical energy storage; calcium hydroxide; calcium oxide; operation modes; low  
15 vapor pressures; thermal charging and discharging

16 **Abstract**

17 The reversible reaction of calcium hydroxide (Ca(OH)<sub>2</sub>) to calcium oxide (CaO) and water vapor is well  
18 known in the context of thermochemical energy storage. Cheap material costs, a theoretically very  
19 high energy density and the potentially wide temperature range of the reaction imply that the  
20 storage system could be beneficial for many high temperature processes. For example the system  
21 could be applied to store and reutilize industrial waste heat or as an alternative storage solution in  
22 future concentrated solar power plants.

23 In this publication the reaction is experimentally investigated in an indirectly operated reactor at  
24 different technically relevant but so far not investigated operating conditions. This in particular  
25 means the thermal charging and discharging of the storage at low water vapor pressures under  
26 different heating and cooling loads induced by a heat transfer fluid. The experiments revealed that  
27 the reaction gas handling not only affects the operating range of the storage but has also a significant  
28 influence on its thermal capability. Especially at low vapor pressures operational limits of the system  
29 have been identified and could be contributed to the effective reaction rate of the unmodified  
30 reaction material which is in the relevant operating range very sensitive to small changes of the local  
31 reaction conditions.

32 **1. Introduction**

33 Thermochemical energy storage by means of the reversible gas solid reaction of calcium hydroxide  
34 (Ca(OH)<sub>2</sub>) to calcium oxide (CaO) and water vapor offers several advantages. Firstly, calcium  
35 hydroxide is a cheap industrial mass product abundantly available all over the world. Secondly, the  
36 enthalpy of reaction is high which leads to high possible energy storage densities. Thirdly, the charge  
37 and discharge temperature of the reaction can theoretically be adapted in a wide range (approx. 300  
38 – 650 °C). Thus the application of the system could potentially be beneficial for many high

39 temperature processes such as the storage and reutilization of industrial waste heat or as an  
40 alternative storage solution in future concentrated solar power plants [1, 2].

41 The reaction system has been examined in many studies but the majority of the studies focus on the  
42 thermal analysis of small sample masses. Already in 1979 Rosemary and his colleagues demonstrated  
43 cycle stability of the reaction for 1171 cycles [3]. Until today different research groups derive kinetic  
44 equations from de- and rehydration experiments carried out in thermogravimetric devices [4-6].  
45 Beyond that other groups focus on the modification of the material in order to adapt the reaction  
46 temperature [7], enhance the reaction rate [8], or improve powder bed properties [9].

47 Besides these investigations on the material level, reports on experiments with lab scale reactors are  
48 scarce. Schaube et al. demonstrated the operation of a fixed bed reactor where the material is in  
49 direct contact with a gas mixture of air and water vapor [10]. Pardo et al. carried out the reaction in a  
50 fluidized bed reactor using a mixture of  $\text{Ca}(\text{OH})_2$  and 70 wt% inert easy to fluidize particles [11]. Yan  
51 et al. recently reported experiments with 400 g of material in a fixed bed set up. They analyzed the  
52 hydration reaction at different vapor pressures but the reactor concept did not allow the recovery of  
53 the released heat. Furthermore the dehydration reaction was driven by an electrical heating jacket  
54 [12].

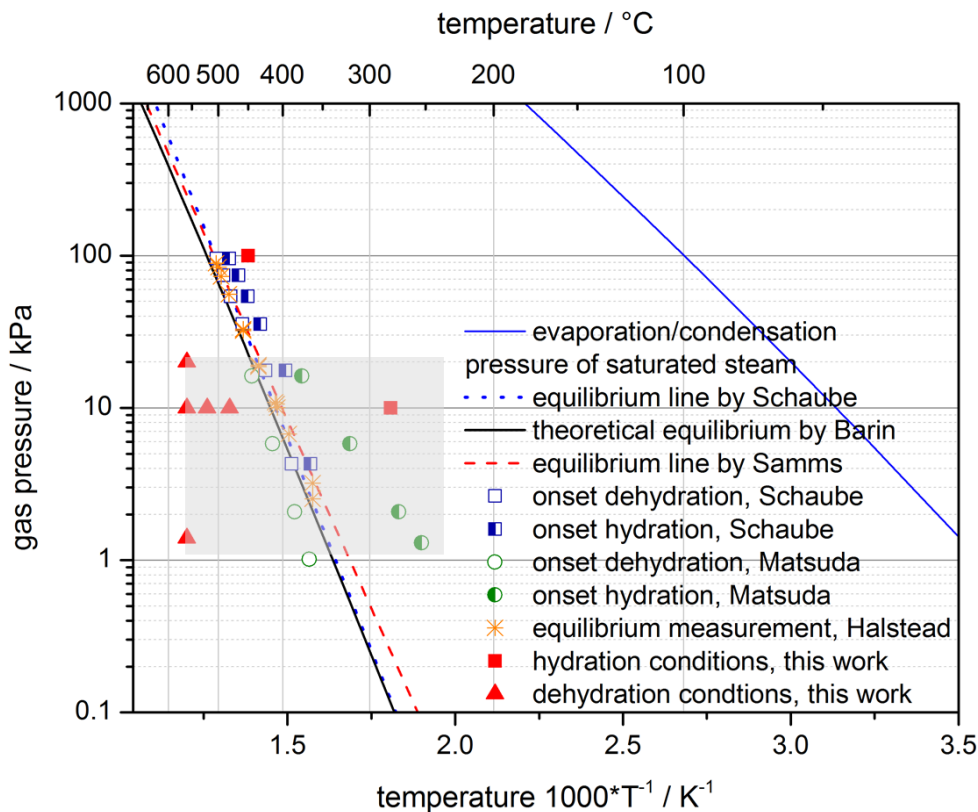
55 All of these concepts have their special advantages and are worth investigating since at the current  
56 state of development an optimal reactor design is not available. However, some process applications  
57 require an indirectly heated concept. For example, if the heat transfer fluid of the process is liquid or  
58 a direct contact of the flue gas and the storage material could cause impurities. In both cases thermal  
59 energy has to be transferred via a heat exchanging surface that separates the reaction from the heat  
60 transfer fluid – a so called indirect concept. An additional advantage of this concept is that the  
61 reaction temperature can be adapted independently from the power output of the reactor. This in  
62 conclusion leads to more flexible operating modes and thus could extend process integration  
63 possibilities.

64 However for indirectly heated reactor concepts there is even less experimental data available. Ogura  
65 et al. were the first who demonstrated a concept where the heat released during the exothermic  
66 reaction was transferred via a heat exchanger to an air flow at ambient temperature [13]. The  
67 dehydration step though was still performed in a furnace. The first concept in which not only the  
68 discharging but also the charging step was driven by an indirect coupling of the reaction bed with a  
69 heat transfer fluid was presented from our group in a previous publication [14]. On one hand the  
70 reactor showed good performance especially for the discharge at reaction gas pressures of 100 kPa  
71 and higher. On the other hand the design of the reaction bed limited the operating range of the  
72 reactor. Particularly at low vapor pressures (e. g. 10 kPa) the performance during charging and  
73 discharging was significantly limited. We mainly contributed this limitation to the mass transfer of  
74 the reaction gas due to the low permeable reaction bed and its height of 200 mm.

75 Nevertheless, as soon as energy efficient process integration is considered, the operation of the  
76 storage system at low vapor pressures is of high technical relevance. There are two main reasons for  
77 that. Firstly, the dehydration at lower vapor pressures results in a lower reaction temperature. As a  
78 consequence we can use lower grade heat to charge the storage. Secondly, the hydration at lower  
79 vapor pressures requires only a reduced evaporation temperature. Therefore the enthalpy of  
80 evaporation can more likely be supplied by waste heat available from the process.

81 Fig. 1 shows the experimentally obtained equilibrium lines of the reaction system  $\text{Ca}(\text{OH})_2/\text{CaO}$  from  
 82 Schaubé [4] and Samms [15] as well as the theoretical equilibrium line based on thermochemical  
 83 values from Barin [16]. In addition reported onset temperatures, determined in thermogravimetric  
 84 measurements from Schaubé [4] and Matsuda [17] are displayed as well as the results of equilibrium  
 85 measurements performed by Halstead [18] in an appropriate test bench. It is obvious that within the  
 86 important operating range for indirect concepts at low vapor pressure (marked as grey area), the  
 87 results vary significantly. This may be on one side contributed to differences in the used material but  
 88 on the other side also the measurement principle itself (e. g. dynamic or static) might have an  
 89 influence.

90 In order to investigate the reaction for thermochemical storage under technically relevant operating  
 91 conditions, we designed a novel reaction bed with minimized mass transfer limitations but a  
 92 sufficient mass of reactive material to investigate thermal capabilities. With this reactor we  
 93 performed several charging and discharging experiments at low vapor pressures and analyzed the  
 94 influence of different heating and cooling loads induced by a heat transfer fluid. The operating  
 95 conditions for the kg-scale experiments presented in this study are marked in Fig. 1 by the red  
 96 red triangles for the dehydration and the red squares for the hydration. For the analysis of the results,  
 97 the experiments in lab-scale were complemented by thermogravimetric measurements in mg-scale  
 98 with the same material.



99

100 **Fig. 1** Thermodynamic equilibrium lines for the  $\text{Ca}(\text{OH})_2/\text{CaO}$  reaction system and operating  
 101 conditions of the performed experiments; evaporation/condensation pressure of saturated steam

## 102 2. Experimental Set Up

### 103 2.1 Reactor

104 The aim of the reaction bed development was to analyze the performance of the storage material for  
105 a wide operating range. The main limitations that are generally contributed to the reactor (not to the  
106 material) are mainly caused by the low permeability and the poor thermal conductivity of the bulk  
107 material. Bearing in mind to minimize these limitations without affecting the material properties we  
108 derived two important design constraints for the novel reactor. First of all, the reaction gas should  
109 only pass through a very thin layer of storage material. Secondly, the furthest distance between a  
110 single particle and the heat exchange surface should be short. Both design constrains would in  
111 principle lead to a very small mass of reaction material. In contrast a representative mass of reaction  
112 material is mandatory, in order to be able to operate the material according to the later application  
113 as thermochemical storage and to allow for both: a proper analysis of the thermal capability of the  
114 reaction and the analysis of the impact of the indirect heating or cooling.

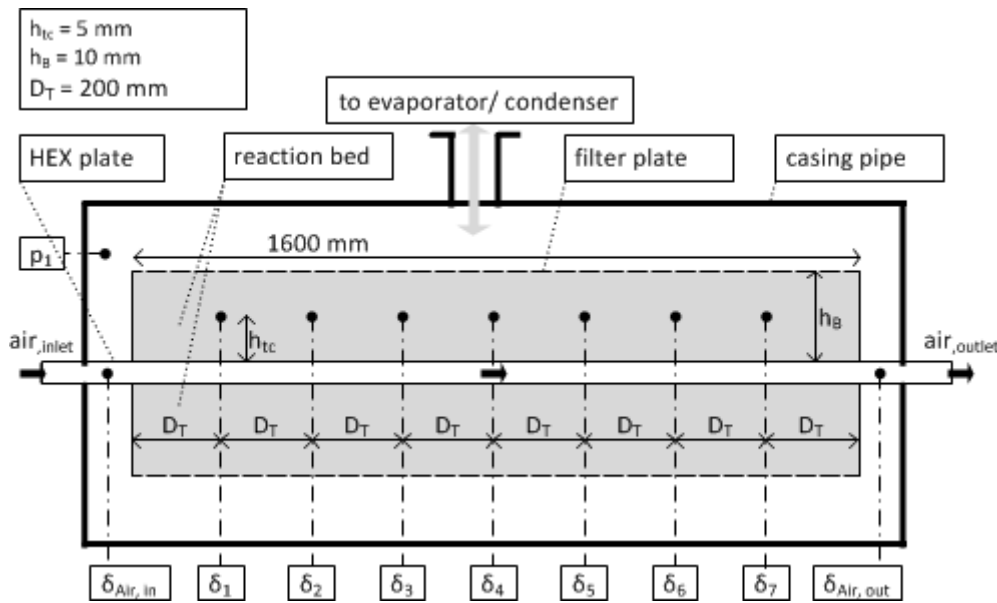
115 Taken all design constraints into account it is obvious that the reactor has to offer a reasonable  
116 compromise between a reactor for investigations and a reactor for thermochemical energy storage.  
117 For this purpose, we choose a single heat exchanger plate as the basis for our reaction bed (see Fig.  
118 1, top). In this concept, the heat transfer fluid, air, flows inside the plate while the storage material  
119 lies on the plate. The plate is on both sides surrounded by a metallic frame of 10 mm height. The  
120 inner sides of the frame measure 150 mm in width and 1600 mm in length giving us 0.48 m<sup>2</sup> heat  
121 exchange surface. Consequently the reactor offers a cubic volume of 4.8 l (2.4 l on each side of the  
122 plate) for the storage material (see Fig 2., bottom left). A gas permeable metallic filter (pore size is 5  
123 μm) placed over the powder material and screwed to the frame encases the reaction bed (see Fig 1.,  
124 bottom right). The large filter area allows for a negligible pressure drop between the powder  
125 material and the reaction gas supply.



126 **Fig. 2** Top: heat exchanger plate used as reactor; bottom left: storage material filled into the frame;  
127 bottom right: filter plate to encase the reaction bed

128 The heat exchanger plate with the encased bed on both sides is mounted into a pressure resistant  
 129 casing pipe. Fig. 3 shows a sectional view of the whole set up including important dimensions and  
 130 positions of the measurement instruments. To observe the reaction progress seven thermocouples  
 131  $\delta_{1-7}$  (type K,  $\pm 0.4 \% X T$ ) are located in the middle of the beds height, at a vertical distance of 5 mm to  
 132 the heat exchange surface. In the horizontal direction of air flow the distance between each  
 133 measurement point is 200 mm with the first point 200 mm away from the beginning of the reaction  
 134 bed. Additional thermocouples measure the air temperature directly at the air in- ( $\delta_{Air,in}$ ) and outlet  
 135 ( $\delta_{Air,out}$ ) of the plate. Furthermore a pressure sensor  $p_1$  (PPA-35XHTT, Keller Ges. für  
 136 Druckmesstechnik mbH,  $\pm 0.8$  kPa) measures the gas pressure in the reaction chamber.

137



138 **Fig. 3** Sectional view of the reaction bed in the casing pipe including important dimension and  
 139 positions of thermocouples and the pressure sensor

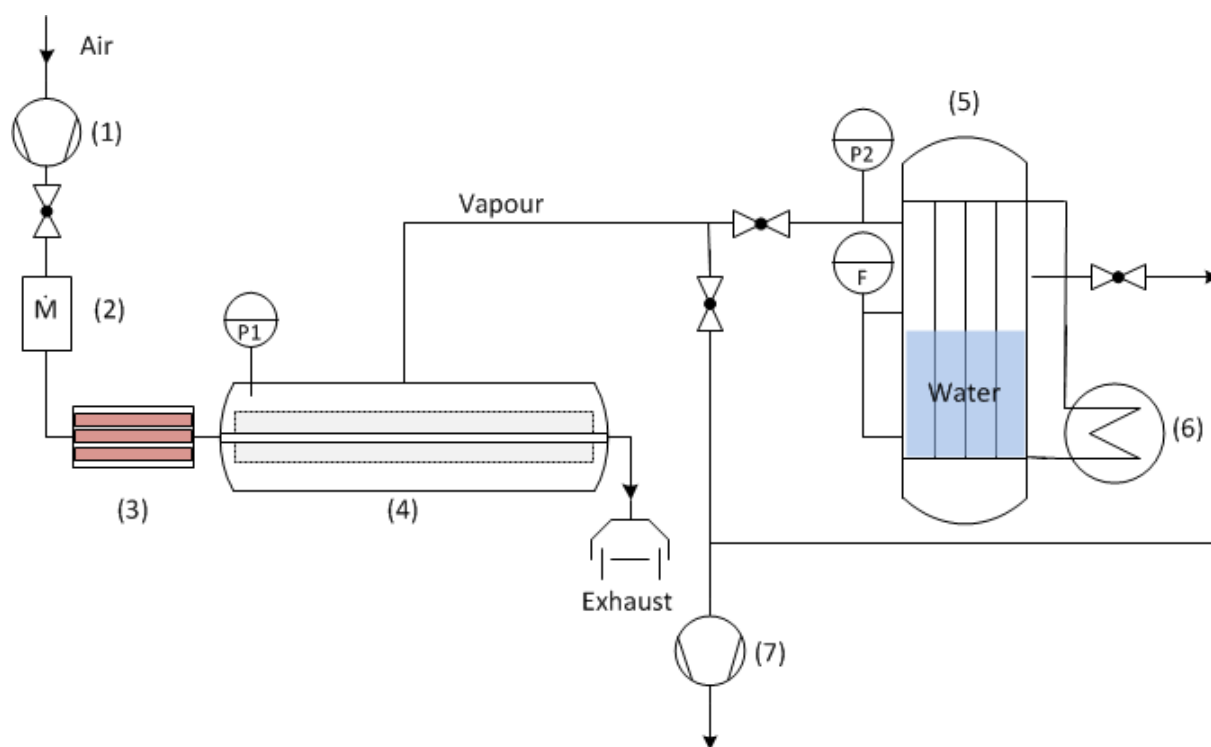
## 140 2.2 Material

141 All experiments presented in this paper we performed with  $Ca(OH)_2$ , product type “Sorbacal®H”,  
 142 supplied by Rheinkalk GmbH/Lhoist group. Based on the products data sheet the purity of the  
 143 material is approximately 98 % the specific surface area is  $19 \text{ m}^2/\text{g}$  and the  $d_{50}$  is  $5.5 \mu\text{m}$ .

## 144 2.3 Test bench

145 Fig. 4 shows the schematic process flow diagram of the test bench. The test bench was designed to  
 146 operate the reactor under different thermal load conditions and at a wide range of vapor pressures.  
 147 Therefore it was most important to be able to adjust the thermal power of the heat transfer fluid and  
 148 the vapor pressure in the reaction chamber independently of each other.

149



150 **Fig. 4** Layout of the test bench

### 151 *Heat transfer fluid supply*

152 Due to the required temperatures, ambient air is used as heat transfer fluid in the experiments and is  
 153 supplied by a compressor (1). The air volume flow can be adjusted with a mass flow controller (2)  
 154 (Bronkhorst, digital flow controller,  $\pm 0.4\%$ ) before it splits up and enters three parallel electrical  
 155 heating units (3). Each heating unit has an electrical power of 2 kW and preheats the air to a  
 156 maximum temperature of 600 °C. After these heating units the air flows merge again in a diminishing  
 157 pipe. This diminishing pipe is equipped with a controllable auxiliary heating to ensure a homogenous  
 158 air temperature at the reactor inlet.

### 159 *Reaction gas handling*

160 During an ongoing reaction we must either remove water vapor from or supply it to the reaction bed.  
 161 To realize this, a tube bundle heat exchanger (5) and a vacuum pump (7) are connected to the  
 162 reactor. With the vacuum pump inert gases are removed from the system ensuring a pure vapor  
 163 atmosphere. The tube bundle heat exchanger operates as condenser or evaporator depending on  
 164 the direction of reaction. A thermal oil flows inside the tubes of the bundle. The oils inlet  
 165 temperature can be tempered between 3-160 °C by a thermostatic bath (6). On the shell side is liquid  
 166 water (for condensation or evaporation) and the water temperature can be kept constant during  
 167 experiments because the thermal oil takes up the heat of condensation or supplies the heat of  
 168 evaporation. Accordingly the evaporation/condensation pressure in the system can be varied  
 169 between 0.7 - 618 kPa and be kept constant during an ongoing reaction. A pressure sensor at the  
 170 outlet flange measures the pressure in the evaporator/condenser and the change of the water level  
 171 is measured with a filling level meter (Vegaflex 65,  $\pm 2$  mm). By means of this value we can monitor  
 172 the reaction and calculate its conversion.

### 173 **2.4 Experimental procedure**

174 For all experiments presented in this paper only one batch of the material described in 2.2 is used. In  
 175 total 2.4 kg are filled in the reactor, equally distributed on each side of the heat exchanger plate.



176 Before every experiment the whole set up is evacuated to  $0.5 \text{ kPa} \pm 0.3 \text{ kPa}$  and afterwards all valves  
 177 are closed. The reactor is preheated to a set starting temperature with the air volume flow and  
 178 additional auxiliary heating cables attached to the casing pipe. Simultaneously we adjust the vapor  
 179 pressure for the experiment in the condenser/evaporator by the thermostatic bath. As soon as the  
 180 pressure in the condenser/evaporator and the temperatures in the reaction bed stay constant an  
 181 experiment can be started.

182 The different operating conditions were shown above (compare Fig. 1). From the equilibrium line for  
 183 water and saturated steam (blue solid line in Fig. 1) the operating temperature of the  
 184 condenser/evaporator at the required pressure can be determined. Besides the different  
 185 temperatures, in some experiments the volume flow of the heat transfer fluid has also been varied.  
 186 The volume flows as well as an overview of all parameters of each presented experiment is given in  
 187 Table 1.

### 188 *Thermal charging procedure (Dehydration)*

189 At the beginning of each dehydration only  $\text{Ca(OH)}_2$  is in the reactor and the set up is preheated to a  
 190 temperature below the equilibrium temperature of the reaction at the adjusted vapor pressure. To  
 191 start the experiment the valve between condenser and reactor is opened and simultaneously the air  
 192 inlet temperature is increased to the set dehydration temperature (marked with red triangles in Fig.  
 193 1). The induced heat load drives the dehydration reaction. Accordingly water vapor comes out of the  
 194 reaction bed and condenses in the condenser. When no further increase of the water level is  
 195 observed the dehydration is finished.

### 196 *Thermal discharging procedure (Hydration)*

197 At the beginning of every hydration experiment only  $\text{CaO}$  is in the reactor and the set up is preheated  
 198 to a set starting temperature (marked with red squares in Fig. 1) below the equilibrium temperature  
 199 of the adjusted evaporation pressure. To start the experiment the valve between reactor and  
 200 evaporator is opened. In that moment water vapor streams into the reaction chamber and initiates  
 201 the exothermic hydration reaction. The air flow takes up the heat of reaction as long as the reaction  
 202 proceeds. The experiment is finished as soon as the temperature in every region of the reaction bed  
 203 has reached its starting value.

204 **Tab. 1** Parameters of all experiments presented in this study

Experiment	$T_{\text{air, initial}} / ^\circ\text{C}$	$\dot{V} / \frac{\text{Nm}^3}{\text{h}}$	$T_{\text{dehydration}} / ^\circ\text{C}$	$P_{\text{condenser/ evaporator}} / \text{kPa}$	$T_{\text{water}} / ^\circ\text{C}$
<b>Dehydration</b>					
A	400	20	560	10	45
B	400	12	560	10	45
C	400	12	520	10	45
D	400	12	480	10	45
E	400	12	560	19.9	60
F	400	12	560	1.4	12
<b>Hydration</b>					
G	280	20	-	8.7	43
H	280	16	-	8.7	43
J	280	12	-	8.7	43
M	450	12	-	100	100

## 205 2.5 Thermogravimetric analysis

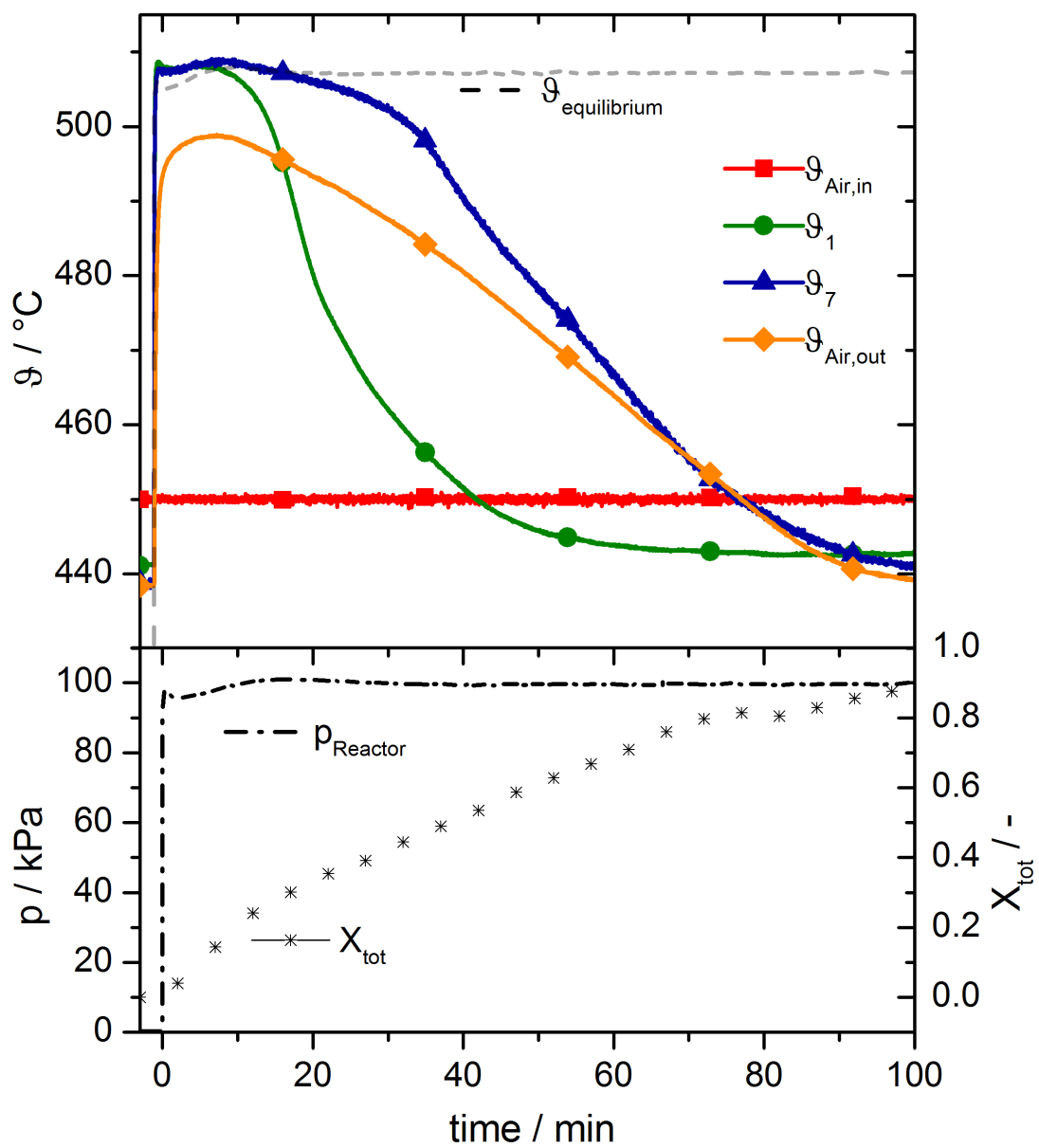
206 To compare some results observed in the reactor a small sample mass (10 mg) of the same batch has  
207 additionally been analyzed in the thermogravimetric analysis (TGA). For these experiments a  
208 NETZSCH simultaneous thermal analysis (STA 449 F3 Jupiter<sup>®</sup>) was used, equipped with a molar  
209 humidity generator (MHG32). The atmosphere during the measurements was inert using nitrogen, or  
210 a mixture of nitrogen and water vapor as purge gas (surrounds the sample) and pure nitrogen as the  
211 protective gas. The pressure inside the furnace was ambient pressure at ~97 kPa and a volume flow  
212 of 100 ml/min of purge gas was used. The bottom of the furnace was heated to 120 °C and a  
213 protection gas volume flow of 20 ml/min nitrogen was supplied, in order to protect the thermo-  
214 balance of condensation drops. The furnace design does not allow the mixing between the purge and  
215 protective gases, thus the protective gas flow does not affect the concentration of humidity inside of  
216 the furnace. With this set up we were able to conduct isothermal hydration and dehydration  
217 experiments in the TGA at vapor pressures comparable to the conditions in the reactor.

## 218 3. Results and Discussions

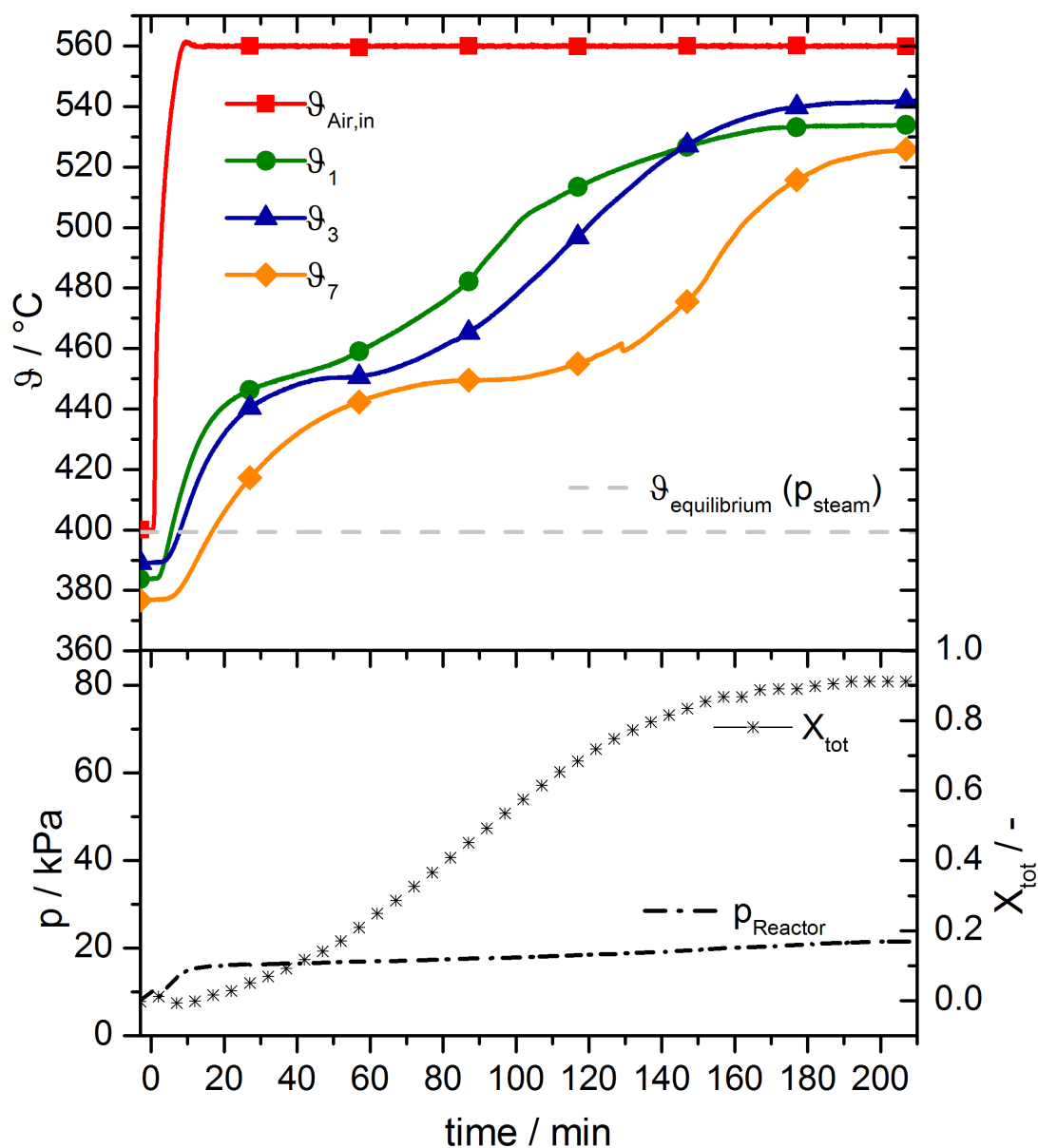
### 219 3.1 Set in operation

220 In order to prove the correct function of the reactor and the measurement equipment a hydration  
221 experiment at an evaporation pressure of 100 kPa according to the procedure as described in 2.5 was  
222 performed.

223 Fig. 5 shows the results of the experiment. We keep the air inlet temperature  $\delta_{\text{Air,in}}$  (red solid line)  
224 constant at 450 °C during the experiment. At  $t = 0$  min we open the valve between evaporator and  
225 reactor thus the pressure in the reactor rises to 100 kPa (black dash dotted line). Consequently the  
226 temperatures in the reaction bed  $\delta_1$  (green solid line) and  $\delta_7$  (blue solid line) jump up to a maximum  
227 of 507 °C. This temperature accords to the theoretical equilibrium temperature (grey dashed line)  
228 which was calculated by the measured pressure and the respective correlation given by Samms et al.  
229 [15] (compare Fig. 1). We also observe a reaction front along the flow direction of the air. Close to  
230 the air inlet the cooling of the reaction bed is maximal due to the largest temperature difference  
231 between the bed and the air. Thus the reaction proceeds quickly and 10 min after the initiation the  
232 temperature  $\delta_1$  drops again. This indicates that a major part of the material is already converted in  
233 this region and the heat released by the reaction decreases. In contrast in the rear region of the  
234 reactor the temperature between the bed and the air flow is small in the beginning. As a  
235 consequence the reaction proceeds slower indicated by the constant temperature plateau which is  
236 hold for 25 min. As more and more material has reacted in this part also the temperature  $\delta_7$  starts to  
237 drop. After 100 min the bed reaches its initial temperature again indicating that no more heat is  
238 released. Accordingly, a conversion of 95 % (black cross dots) is measured at this time. The Difference  
239 before and after the reaction between air inlet temperature and temperatures inside the reaction  
240 bed are contributed to radiative heat losses inside the reaction chamber, that have been minimized  
241 but cannot be completely removed.



242 **Fig. 5** Hydration experiment at 100 kPa and a starting temperature of 450 $^{\circ}\text{C}$



244 **Fig. 6** Dehydration experiment at 10 kPa and a dehydration temperature of 560 °C

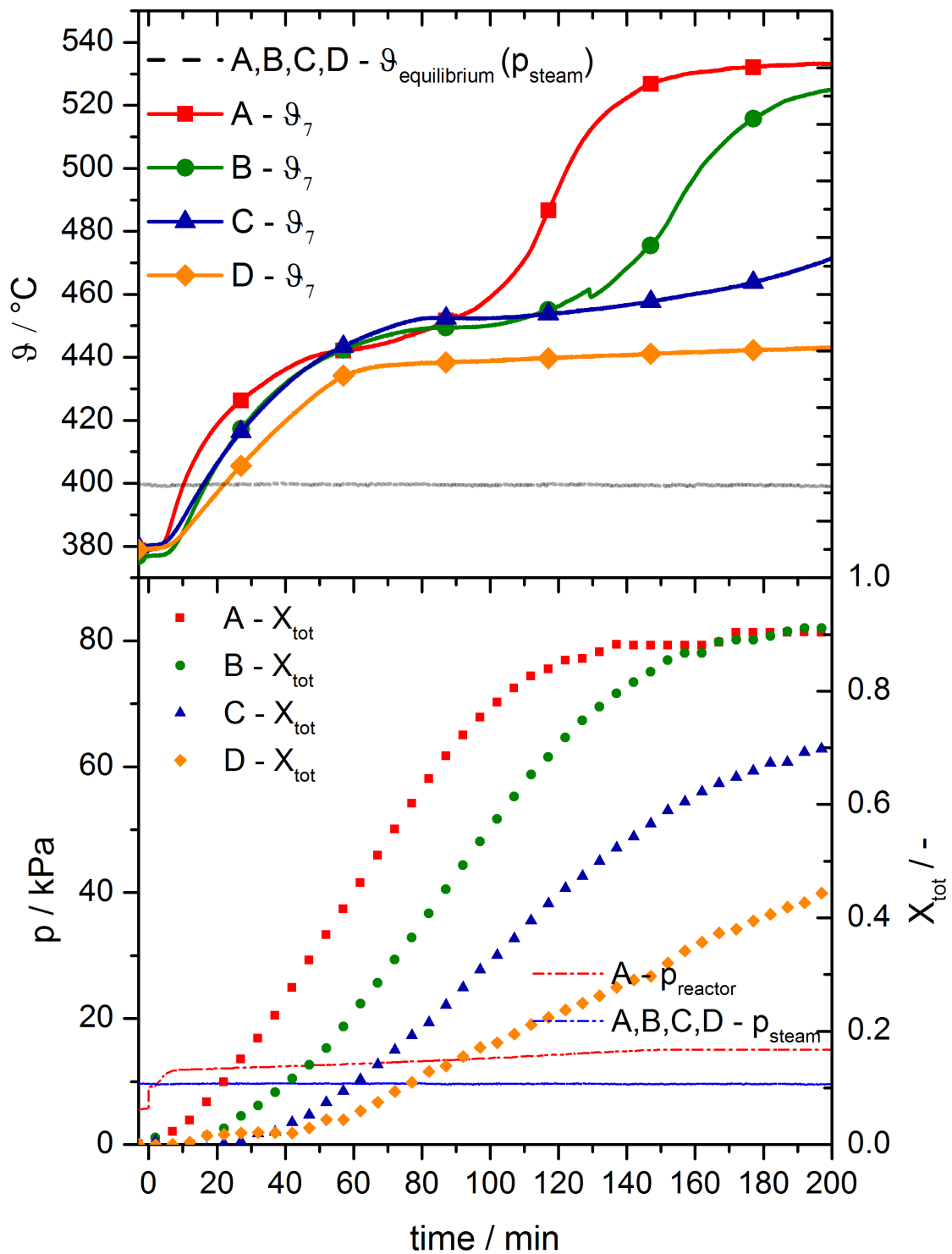
245 A reference dehydration experiment has been performed with a preheating temperature of 400 °C  
 246 and a condensation pressure of 10 kPa (condensation temperature 45 °C). Fig. 6 shows the  
 247 temperature, pressure and conversion trends. At  $t = 0$  min the air inlet temperature starts to rise up  
 248 to the set dehydration temperature of 560 °C (red solid line). Exemplarily the temperatures  $\delta_1$  (green  
 249 solid line)  $\delta_3$  (blue solid line) and  $\delta_7$  (orange solid line) positioned in the front, middle, and rear region  
 250 (compare Fig.2) of the bed are plotted. Within the first 30 min the material temperatures increase to  
 251 445 °C due to the incoming heat flux. At a temperature of 445 °C a significant change occurs in the  
 252 slope of the temperature trend. In particular in the middle ( $\delta_3$ ) and rear region ( $\delta_7$ ) of the bed a  
 253 temperature plateau can be observed. The temperature plateau indicates that the heat input from  
 254 the heat transfer fluid is completely absorbed by the endothermic reaction. Accordingly during this

255 time we also observe that the conversion trend (black cross dots) shows a constant rate indicating  
256 the ongoing reaction with a constant thermal charging power. After 120 min almost 80 % of the  
257 material is converted thus the heat input in the rear region slowly becomes larger than the amount  
258 of heat which is still absorbed by the endothermic reaction. Consequently the material temperature  
259 rise again until after 200 min a conversion of 96 % is reached and all bed temperatures reach their  
260 constant maximum. What might seem controversy is that the temperature plateau lies at 445 °C  
261 while the equilibrium temperature at the condensation pressure of 10 kPa is 400 °C (grey dash  
262 dotted line). This significant distance to the theoretical equilibrium temperature was further analyzed  
263 with a variation of thermal power of the heat transfer fluid.

#### 264 *Variation of heat load of the heat transfer fluid*

265 In order to analyze the influence of the thermal power of the heat transfer fluid on the dehydration  
266 reaction, we performed the dehydration experiments at a condensation pressure of 10 kPa with 4  
267 different thermal heat fluxes into the reaction bed. The results are shown in Fig. 7. Experiment A (red  
268 curves) runs with a 60 % higher volume flow than the reference experiment B (green curves) but with  
269 the same dehydration temperature of 560 °C. Experiment C (blue curves) and D (orange curves) run  
270 with the nominal volume flow but at reduced dehydration temperatures of 520 °C respectively 480  
271 °C (compare Table 1. for all parameters). The conversion curves show that the influence of the heat  
272 flux into the bed directly correlates with the speed of conversion. With the largest heat flux we  
273 receive the shortest dehydration time (red squares – experiment A), whereas smaller heat fluxes  
274 prolong the dehydration times (B, C, D).

275 Fig. 7 also shows the temperature trend of  $\delta_7$  for every experiment. We can see that independently  
276 from the heat flux into the bed, the material temperatures increase within the first 30 min. This  
277 indicates that initially the reaction speed is so slow that the incoming heat flux is larger than the  
278 thermal energy absorbed by the reaction. However a constant temperature plateau develops at  
279 temperatures above 440 °C for all experiments. In general, a temperature plateau region during  
280 dehydration is characterized by an equilibrium state between the thermal energy absorbed by the  
281 endothermic reaction and the heat flux delivered by the heat transfer fluid. It is remarkable that in  
282 the experiments A, B and C the plateau lies at the same temperature of 445 °C independently of the  
283 heat flux into the reaction bed. This supports the hypothesis of a limitation that is due to material  
284 intrinsic properties which in turn would lead to a serious limitation of the operating range of this  
285 thermochemical storage: In contrast to the hydration experiment at 100 kPa (compare Fig. 5) where  
286 the operating range can be basically derived from the equilibrium line, the measured plateau  
287 temperature of 445 °C for these experiment is around 45 K higher than the value predicted by the  
288 equilibrium line. Only in experiment D the plateau temperature is slightly lower at 440 °C - but at the  
289 same time the charging power seems not anymore of technical relevance due to its long dehydration  
290 time. In order to further analyze this important aspect for the operation flexibility of a  
291 thermochemical energy storage based on  $\text{Ca}(\text{OH}_2)$ , we performed additional experiments by  
292 thermogravimetric analysis.

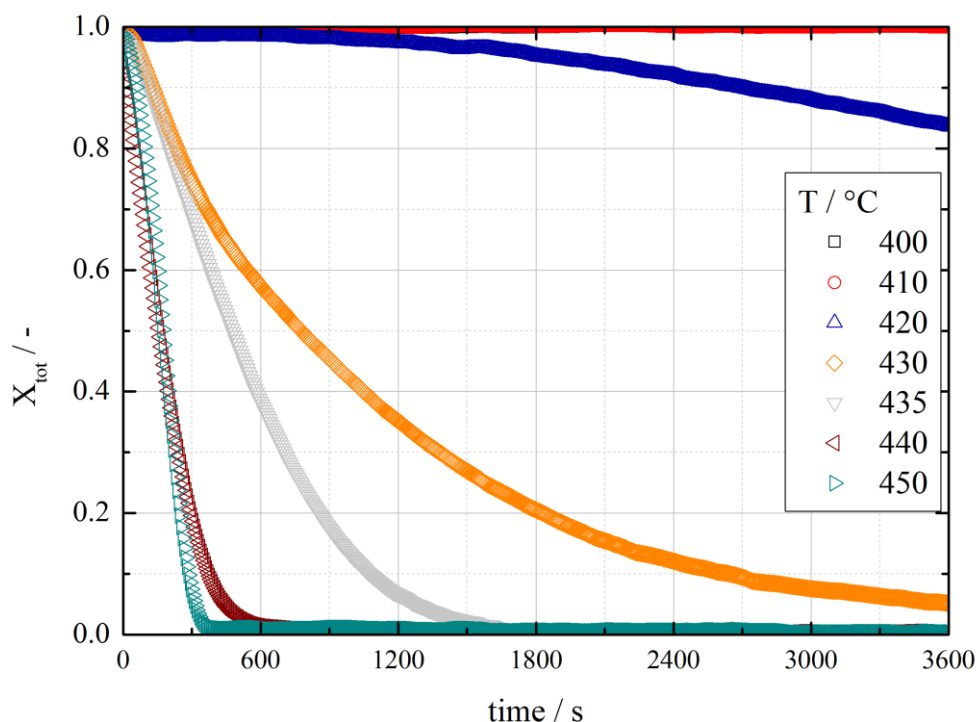


293 **Fig. 7** Dehydration experiments at 10 kPa at different heat loads of the heat transfer fluid

295 **Dehydration at 10 kPa in the TGA**

296 The experiments in the TGA were performed according to the procedure described in 2.6 and  
297 conditions comparable to the reactor experiments. The main differences to generally reported TGA  
298 data for Ca(OH)<sub>2</sub> are isothermal measurement conditions at very low gas pressures. Seven different  
299 dehydration experiments at a humid atmosphere inside the furnace of 10 kPa and isothermal  
300 temperatures between 400 °C and 450 °C were conducted. Each temperature was remained constant  
301 for 1 hour while the mass change was measured.

302



303

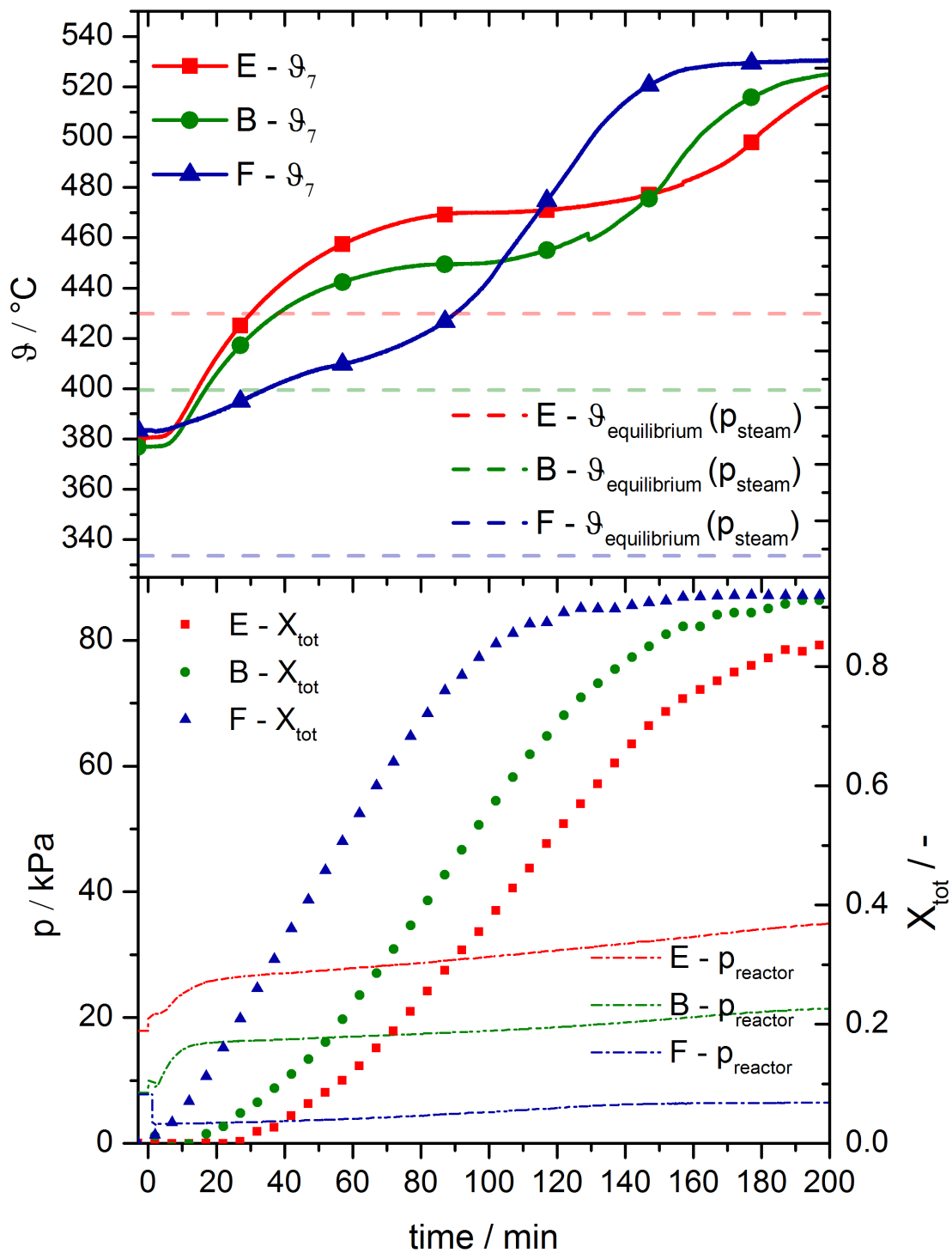
304 **Fig. 8** Effect of the temperature on the dehydration reaction of Ca(OH) at a vapor pressure of 10 kPa

305 Fig. 8. shows the conversion trend of Ca(OH)<sub>2</sub> to CaO at different isothermal measurements. It can be  
306 observed that at 400 °C and 410 °C no mass change occurs within 1 hour. At 420 °C a small mass  
307 change was measured, while at 430 °C the rate of conversion changes significantly but conversion is  
308 still incomplete after 1 hour. At 435 °C we reach full conversion after 30 min - but with only a slight  
309 increase of 5 K to 440 °C the dehydration time is reduced to less than 10 min. A further increase to  
310 450 °C does not result in a significantly faster conversion.

311 The results from the thermogravimetric analysis accord to what was observed in the reactor. Below a  
312 temperature of 440 °C the reaction rate is rather slow thus the heat flux into the reaction bed is  
313 always higher than the thermal energy absorbed by the reaction. As a consequence the reaction bed  
314 heats up sensible. When we exceed 440 °C the reaction becomes so fast that the heat flux into the  
315 reaction bed is completely absorbed by the endothermic reaction. Consequently a constant  
316 temperature plateau forms. With regard to a later application of Ca(OH)<sub>2</sub> as thermochemical storage,  
317 it can be concluded that the unmodified material possesses a kind of tipping point: at a condensation

318 pressure of 10 kPa (corresponding to a condensation temperature of 45 °C) a charging temperature  
 319 of at least 445 °C is required to achieve technically relevant charging times (less than two hours).

320 *Variation of condensation pressure*



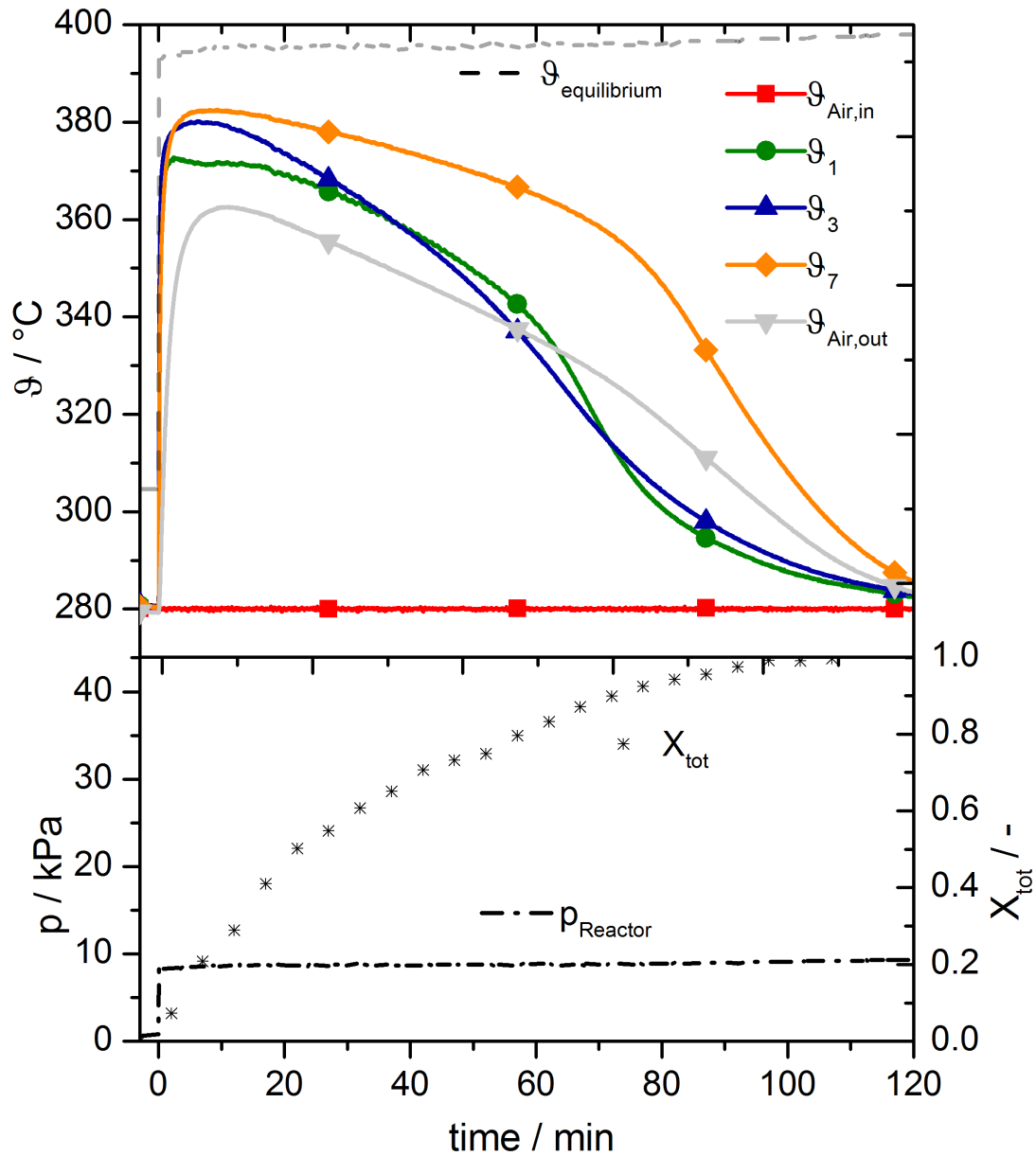
321

322 **Fig. 9** Dehydration experiments at 1.4, 10 and 20 kPa and a dehydration temperature of 560 °C



323 In order to examine the influence of the condensation pressure on the dehydration time and the  
324 charging temperature we performed experiments at three different condensation pressures but at  
325 the same heat load induced by the heat transfer fluid. Experiment B (green line) is the reference  
326 dehydration experiment at 10 kPa while experiment E (red line) is performed at 20 kPa and  
327 experiment F (blue line) is performed at 1.4 kPa. Each experiment was run with the nominal volume  
328 flow and the air inlet temperature was increased to 560 °C. From the conversion curves we can  
329 clearly see, that the lower the condensation pressure the faster we reach full conversion. For  
330 example for experiment F 80 % is converted after 80 min while for experiment B 80 % conversion is  
331 achieved in 120 min, respectively in 180 min for experiment E.

332 Even more interesting are the plotted temperature trends for the rear region of the bed. We can see  
333 that for the experiments at 10 kPa and 20 kPa the temperature trends are qualitatively similar. The  
334 material heats up sensible in the beginning until the reaction becomes as fast that we reach an  
335 equilibrium state between heat influx into the reaction bed and the thermal energy absorbed by the  
336 reaction (indicated by the constant temperature plateaus). In all cases we observe that the above  
337 discussed temperature difference to the theoretical equilibrium temperature (red, green and blue  
338 dashed line) is required. However the difference tends to be smaller for higher dehydration  
339 pressures: the difference is 35 K at 20 kPa, 45 K at 10 kPa and more than 50 K for 1.4 kPa (compare  
340 Fig. 9). But even though a smaller temperature difference to the equilibrium is required at 20 kPa the  
341 dehydration temperature at which reasonable reaction rates can be realized is already 465 °C. From  
342 a process integration point of view this means energy at a higher temperature is required to charge  
343 the storage. If the condensation pressure is lower the dehydration can be performed faster and at  
344 lower temperatures which would be favorable for the integration of the storage system (lower  
345 charging temperatures are required). However it must be taken into account that a lower  
346 condensation pressure might require an additional cooling load for the condenser.



348 **Fig. 10** Hydration experiment at 8.7 kPa and a starting temperature of 280 °C

349 Fig. 10 shows a reference experiment for the thermal discharging. The initial temperature was set to  
 350 280 °C and the evaporator was tempered at 43 °C. At min 0 the valve between evaporator and  
 351 reactor is opened and the pressure in the reactor increases to ~8.7 kPa (compare black dash dotted  
 352 line in Fig. 10). In the moment when the vapor enters the reactor the bed temperatures escalate  
 353 (compare  $\delta_1$ ,  $\delta_3$  and  $\delta_7$  in Fig. 10) due to the heat released by the exothermic reaction. It seems that in  
 354 the front ( $\delta_1$ ) and middle region ( $\delta_3$ ) of the bed the temperatures reach slightly lower maxima than in  
 355 the rear region ( $\delta_7$ ). This can be ascribed to the higher cooling load of the reaction bed closer to the  
 356 air inlet where the temperature difference between bed and the incoming air is maximal.

357 In the rear region the temperature in the bed reaches a maximum of  $\sim 383$  °C and stays constant for  
358 approximately 20 min. In contradiction to the discharging experiment at 100 kPa (compare Fig. 5), in  
359 this case, at lower vapor pressures, a deviation of the plateau temperature from the equilibrium line  
360 of 15 K is observed. Since it is lower than the theoretical equilibrium temperature of the reaction  
361 (grey dashed line) one could dedicate this observation again to the reaction rate at given conditions:  
362 Initially, at the beginning of the experiment, the rate of reaction is high since the temperature  
363 difference between the start temperature of 280 °C and the theoretical equilibrium temperature of  
364 398 °C is large. As a consequence more heat is released by the exothermic reaction than removed by  
365 the heat transfer fluid which leads in turn to increasing temperatures. The increasing temperature  
366 directly leads to a deceleration of the reaction rate. In contrast to the reference experiment at 100  
367 kPa, at lower vapor pressure the deceleration of the heat release seems more pronounced since the  
368 temperature predicted by the theoretical equilibrium line is in this case not reached.

### 369 **Variation of cooling load of the heat transfer fluid**

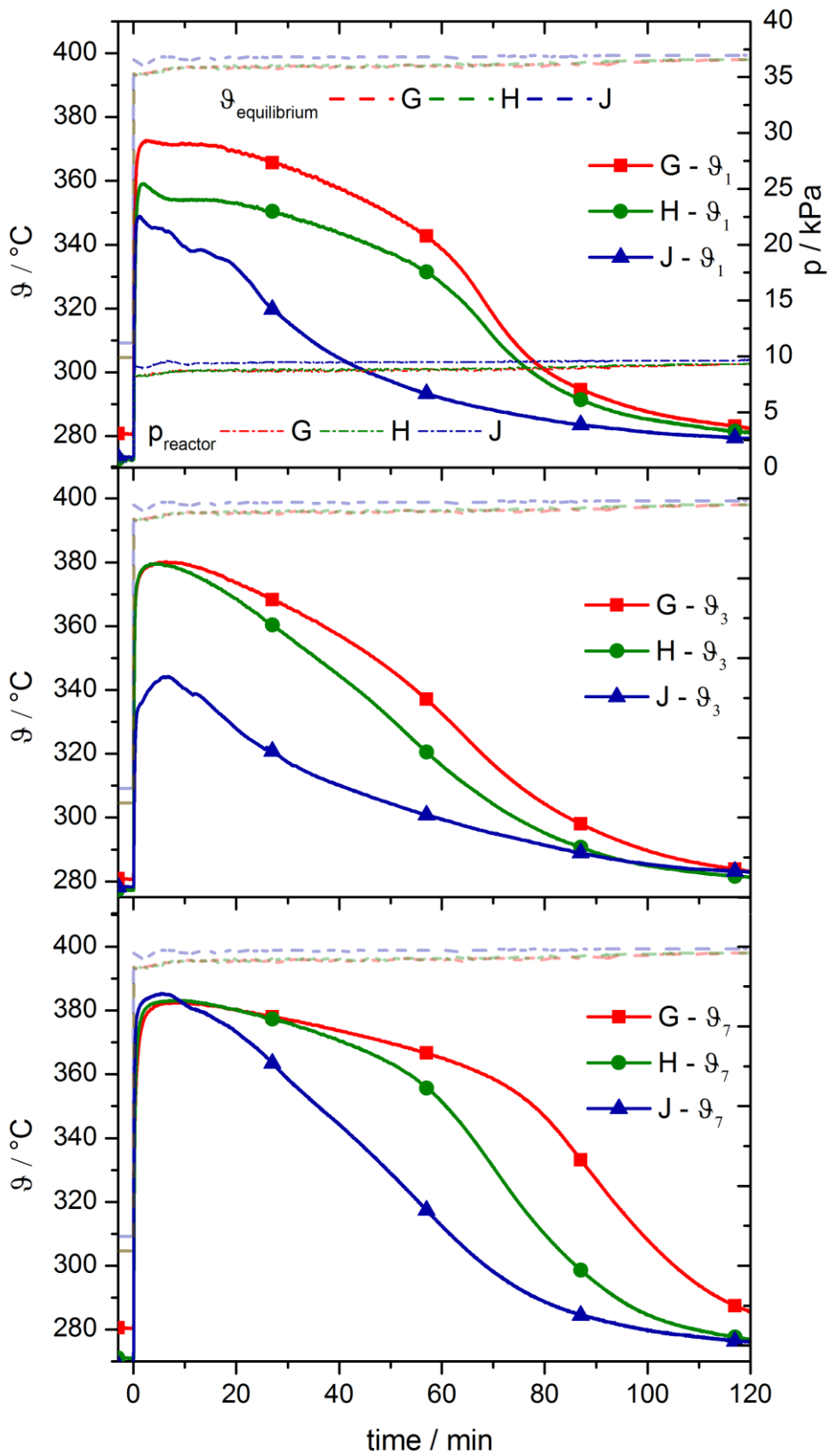
370 To analyze the influence of different cooling loads on the discharge temperature experiments at  
371 three different volume flows of the heat transfer fluid have been conducted. The results are shown in  
372 Fig. 11. Experiment G (red solid lines) was run with the nominal volume flow of 12 Nm<sup>3</sup>/h while in the  
373 experiments H (green solid line) and J (blue solid line) the volume flow was increased to 16 Nm<sup>3</sup>/h  
374 and 20 Nm<sup>3</sup>/h. In all cases the air inlet temperature was set to 280 °C and the exothermic reaction  
375 was induced by a gas pressure of 8.7 kPa. The temperature trends in the front ( $\delta_1$ ), middle ( $\delta_3$ ) and  
376 rear region ( $\delta_7$ ) of the bed are plotted.

377 In particular in the front region of the reaction bed (compare  $\delta_1$ , first diagram of Fig. 11) the reached  
378 temperatures directly correlate with the volume flow of the heat transfer fluid, respectively the  
379 cooling load of the reaction bed. The experiment with the highest cooling load shows the lowest  
380 temperature maximum of  $\sim 350$  °C (blue curve). Whereas the experiment with the medium cooling  
381 load (green curve) shows a kind of plateau at  $\sim 355$  °C and a clear temperature plateau lies at 370 °C  
382 for the experiment with the lowest cooling load (red curve). Again, temperature plateaus indicate an  
383 equilibrium state between the heat released due to the exothermic reaction and the heat taken up  
384 by the heat transfer fluid. Closer to the equilibrium temperature the reaction decelerates thus less  
385 heat is released. Accordingly the plateau for lower cooling loads is at higher temperatures. If the  
386 cooling load increases, the temperature plateau arises at lower temperatures, since at temperatures  
387 further away from the equilibrium temperature, the reaction rate accelerates. This trend can be  
388 observed in the first diagram of Fig. 11 even though the experiment with the highest cooling load  
389 (blue) reaches rather a peak than a plateau.

390 In the middle region of the reactor ( $\delta_3$ , second diagram Fig. 11) we observe that the material  
391 temperature for the experiment with the highest cooling load still remains below 350 °C while for the  
392 other two experiments the same maximum temperature of 380 °C is reached. In the rear region of  
393 the reactor ( $\delta_7$ ) the same maximum temperature of around 380 - 383 °C is reached for all  
394 experiments. At this position the temperature difference between the reaction and the heat transfer  
395 fluid is rather small since the heat exchange takes first place in the front and later in the middle  
396 region of the reactor. However, still the maximum temperature is approximately 15 K below the  
397 thermal equilibrium.

398 Since for these experiments, the inlet temperature was kept constant, the temperature difference  
399 between the reaction and heat transfer fluid was generated by the exothermic reaction itself. In

400 contrast to physical storages, in this case a high local heat flux is characterized by a reaction at a  
401 lower temperature level (compare values for highest heat flux at the front region). Consequently,  
402 one can conclude that this leads in turn to an optimization question for the later application of the  
403 thermochemical storage: for low vapor pressures, high power densities directly reduce the quality  
404 (temperature level) of the discharged thermal energy. Additionally, comparable to the charging  
405 experiments, a material intrinsic tipping point seems to limit the maximum reaction temperature at  
406 8.7 kPa to around 15 K below the theoretical equilibrium. To investigate this hypothesis additional  
407 isothermal hydration experiments have been conducted by TGA.



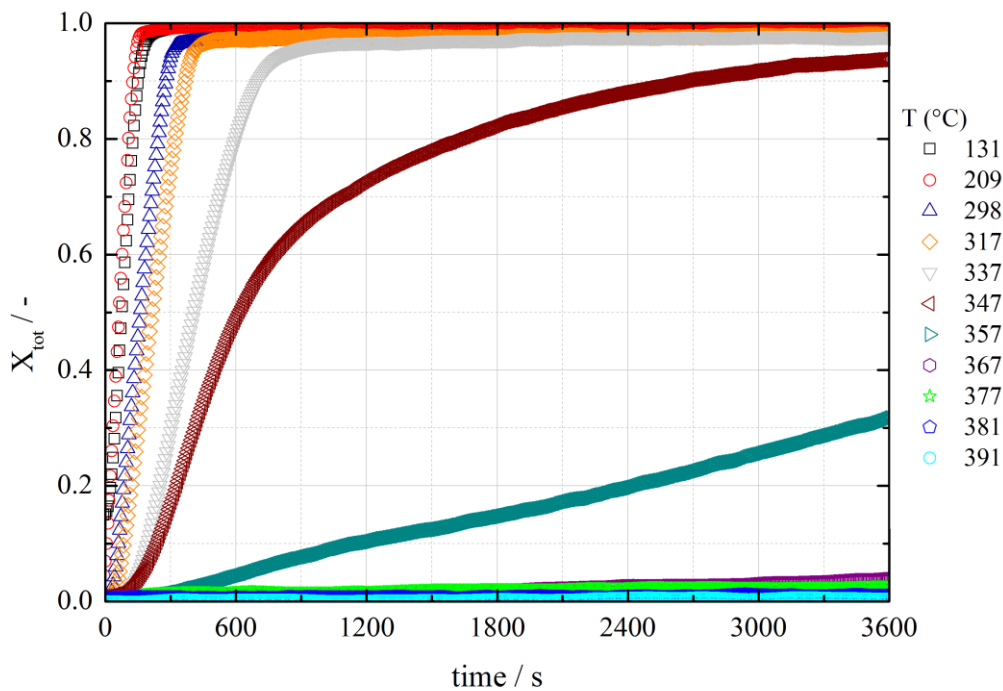
408 **Fig. 11:** Hydration experiments at 8.7 kPa under different cooling loads of the heat transfer fluid

409 **Hydration at 8.7 kPa in the TGA**

410 To support the findings observed in the reactor we examined the rate of reaction under comparable  
411 operating conditions in the thermogravimetric analysis. Before every hydration cycle,  $\text{Ca(OH)}_2$  was  
412 dehydrated under nitrogen atmosphere. The hydration experiments were performed at a water  
413 vapor pressure of 8.7 kPa and at different isothermal temperatures between 390 °C and 110 °C. The  
414 hydration temperature was reduced about 10 K in each following cycle.

415 Fig. 12 shows the conversion trends for the experiments. We can see that for temperatures between  
416 391 °C (theoretical equilibrium is 398 °C) and 367 °C almost no material has reacted after one hour.  
417 At 357 °C approximately 30 % of the material is hydrated after 1 hour while at 347 °C almost 80 % is  
418 hydrated within the first 20 min. At a temperature of 337 °C we achieve 80 % of conversion within 10  
419 min while at temperatures below 300 °C the conversion accelerates only slightly.

420 One can conclude that at temperatures above 360 °C the rate of reaction is rather slow while at  
421 temperatures below 350 °C the rate of reaction quickly accelerates. Consequently, one can state that  
422 the tipping point for a technically relevant discharge reaction of the  $\text{Ca(OH)}_2$  with a vapor pressure of  
423 8.7 kPa (corresponding to an evaporation temperature of 43 °C) is at around 350 °C. This value is  
424 around 48 K below the theoretical discharge temperature according to the equilibrium line.



425

426 **Fig. 12** Effect of the temperature on the hydration reaction of CaO at a gas pressure of 8.7 kPa

427 **4. Conclusions**

428 This study presents a newly designed indirectly heated reaction bed for 2.4 kg of calcium hydroxide  
429 storage material. The reactor design was especially dedicated to investigate the reaction at low vapor  
430 pressures and under different thermal loads induced by the heat transfer fluid.

431 Thermal charging and discharging at technically relevant operating conditions were experimentally  
432 demonstrated at vapor pressures between 1.4 kPa and 20 kPa. It can be stated that the operation of  
433 the storage system at low vapor pressures is possible. This not only enhances process integration  
434 possibilities (gas handling) but could also increase the overall storage efficiency of the  
435 thermochemical system. However, the experiments revealed that the operating range of the calcium  
436 hydroxide system is partially limited due to the effective reaction rate of the storage material at low  
437 vapor pressure. For example for the thermal charging at 10 kPa (condensation at 45 °C) a technically  
438 relevant minimum temperature of 445 °C was identified which is around 45 K higher compared to the  
439 theoretical values. For the discharge at 8.7 kPa (evaporation at 43 °C) a maximum temperature of  
440 only 383 °C could be reached which is 15 K below the theoretical value. However for high discharge  
441 powers a reaction temperature below 350 °C should be maintained during the discharge process. For  
442 process integration studies as well as evaluations of Ca(OH)<sub>2</sub> as thermochemical energy storage, this  
443 limited operating range at low water pressures has to be taken into account. Further studies will  
444 complement the technically relevant operation range of Ca(OH)<sub>2</sub> for higher vapor pressures.

445

446

447 **References**

- 448 [1] Schaub F, Wörner A, Tamme R. High Temperature Thermochemical Heat Storage for  
449 Concentrated Solar Power Using Gas–Solid Reactions. *J. Sol. Energy Eng.* 2011;133.  
450 doi:10.1115/1.4004245.
- 451 [2] Prieto C, Cooper P, Fernández AI, Cabeza LF. Review of technology: Thermochemical energy  
452 storage for concentrated solar power plants. *Renew. Sustain. Energy Rev.* 2016;60:909–29.  
453 doi:10.1016/j.rser.2015.12.364.
- 454 [3] Rosemary JK, Bauerle GL, Springer TH. Solar Energy Storage Using Reversible Hydration-  
455 Dehydration of CaO-Ca(OH)<sub>2</sub>. *J. Energy* 1979;3:321–322.
- 456 [4] Galwey AK, Lavery GM. A kinetic and mechanistic study of the dehydroxylation of calcium  
457 hydroxide. *Thermochim. Acta* 1993;228:359–78. doi:10.1016/0040-6031(93)80304-S.
- 458 [5] Schaub F, Koch L, Wörner A, Müller-Steinhagen H. A thermodynamic and kinetic study of the de-  
459 and rehydration of Ca(OH)<sub>2</sub> at high H<sub>2</sub>O partial pressures for thermo-chemical heat storage.  
460 *Thermochim. Acta* 2012;538:9–20. doi:10.1016/j.tca.2012.03.003.
- 461 [6] Criado YA, Alonso M, Abanades JC. Kinetics of the CaO/Ca(OH)<sub>2</sub> Hydration/Dehydration Reaction  
462 for Thermochemical Energy Storage Applications. *Ind. Eng. Chem. Res.* 2014;53:12594–601.  
463 doi:10.1021/ie404246p.
- 464 [7] Shkatulov A, Aristov Y. Modification of magnesium and calcium hydroxides with salts: An efficient  
465 way to advanced materials for storage of middle-temperature heat. *Energy* 2015.  
466 doi:10.1016/j.energy.2015.04.004.
- 467 [8] Kariya J, Ryu J, Kato Y. Development of thermal storage material using vermiculite and calcium  
468 hydroxide. *Appl. Therm. Eng.* 2016;94:186–92. doi:10.1016/j.applthermaleng.2015.10.090.  
469
- 470 [9] Roßkopf C, Afflerbach S, Schmidt M, Görtz B, Kowald T, Linder M, et al. Investigations of nano  
471 coated calcium hydroxide cycled in a thermochemical heat storage. *Energy. Convers. Manag.*  
472 2015;97:94–102. doi:10.1016/j.enconman.2015.03.034.  
473
- 474 [10] Schaub F, Kohzer a., Schütz J, Wörner a., Müller-Steinhagen H. De- and rehydration of Ca(OH)<sub>2</sub>  
475 in a reactor with direct heat transfer for thermo-chemical heat storage. Part A: Experimental results.  
476 *Chemical Engineering Research and Design* 2013;91:856–64. doi:10.1016/j.cherd.2012.09.020.  
477
- 478 [11] Pardo P, Anxionnaz-Minvielle Z, Rougé S, Cognet P, Cabassud M. Ca(OH)<sub>2</sub>/CaO reversible  
479 reaction in a fluidized bed reactor for thermochemical heat storage. *Solar Energy* 2014;107:605–16.  
480 doi:10.1016/j.solener.2014.06.010.  
481
- 482 [12] Yan J, Zhao CY. Experimental study of CaO/Ca(OH)<sub>2</sub> in a fixed-bed reactor for thermochemical  
483 heat storage. *Applied Energy* 2016;175:277–84. doi:10.1016/j.apenergy.2016.05.038.  
484
- 485 [13] Ogura H, Yamamoto T, Kage H. Effects of heat exchange condition on hot air production by a  
486 chemical heat pump dryer using CaO/H<sub>2</sub>O/Ca(OH)<sub>2</sub> reaction. *Chemical Engineering* 2002;86:3–10.  
487
- 488 [14] Schmidt M, Szczukowski C, Roßkopf C, Linder M, Wörner A. Experimental results of a 10 kW high  
489 temperature thermochemical storage reactor based on calcium hydroxide. *Applied Thermal*  
490 *Engineering* 2014;62:553–9. doi:10.1016/j.applthermaleng.2013.09.020.



- 491  
492 [15] Samms AC, Evans BE. THERMAL DISSOCIATION OF Ca (OH)<sub>2</sub>, AT ELEVATED PRESSURES 1968;18.
- 493 [16] I. Barin, Thermochemical Data of Pure Substances, VCH Verlagsgesellschaft, Weinheim, 1993
- 494 [17] H. Matsuda, T. Ishizu, S.K. Lee, M. Hasatani, Kinetic study of Ca(OH)<sub>2</sub>/CaO reversible  
495 thermochemical reaction for thermal energy storage by means of chemical reaction, Kagaku Kogaku  
496 Ronbunshu 1985;11;542–548.
- 497 [18] Halstead PE, Moore AE. 769. The thermal dissociation of calcium hydroxide. Journal of the  
498 Chemical Society (Resumed) 1957;3873. doi:10.1039/jr9570003873.
- 499

500 **Nomenclature**

501 HEX heat exchanger

502 TGA thermogravimetric analysis

503 P pressure

504 T temperature

505 t time

506  $\delta$  temperature measurement point, thermocouple

507  $\dot{V}$  volume flow

508 X conversion

509